

SBF distances to Leo and Virgo using the HST^{*}.

P.W. Morris¹ and T. Shanks¹

¹ *Department of Physics, Durham University, South Road, Durham, DH1 3LE.*

Accepted- . Received ; in original form

ABSTRACT

We have used archive HST WFPC2 data for three elliptical galaxies (NGC 3379 in the Leo I group, and NGC 4472 and NGC 4406 in the Virgo cluster) to determine their distances using the Surface Brightness Fluctuation (SBF) method as described by Tonry and Schneider (1988). A comparison of the HST results with the SBF distance moduli of Ciardullo et al (1993) shows significant disagreement and suggests that the r.m.s. error on these ground-based distance moduli is actually as large as ± 0.25 mag. The agreement is only slightly improved when we compare our results with the HST and ground-based SBF distances from Ajhar *et al* (1997) and Tonry *et al* (1997); the comparison suggests that a lower limit on the error of the HST SBF distance moduli is ± 0.17 mag. Overall, these results suggest that previously quoted measurement errors may underestimate the true error in SBF distance moduli by at least a factor of 2-3.

Key words: distance scale — galaxies: distances and redshifts — galaxies: photometry — galaxies: individual (NGC 3379, NGC 4406, NGC 4472)

1 INTRODUCTION

There now exist several methods of distance determination that appear to give measurements with small errors, *i.e.* the SBF method and the use of planetary nebula luminosity function (PNLF). Both of these methods claim (and appear to deliver) distances with an accuracy of better than 10%. These methods are crucial in determining the zero-point and reliability of other distance estimators and also in determining the structure of the Universe in our neighbourhood out to about 30Mpc.

In this paper we present an analysis of archive HST WFPC2 data of three ellipticals using the SBF method. The SBF method is based on the pixel-to-pixel brightness variations that are present in all galaxies, which is due to the varying number of stars within each pixel. The variations are proportional to $\bar{f}\sqrt{N_*}$ where \bar{f} is the mean flux of a star and N_* is the average number of stars per pixel. To detect the SBF signal, it must be strong enough to be separated from sources of noise within the frame. The main sources of noise are shot noise and contamination from faint objects within the frame. The shot noise can be overcome by taking a long enough exposure, but the contamination from point

Galaxy	P.I.	Proposal ID	F814W	F555W
NGC 3379	Faber	5512	3x500,1x160	3x400,1x140
NGC 4472	Westphal	5236	2x900	2x900
NGC 4406	Faber	5512	3x500	3x500

Table 1. HST archive data used for the SBF analysis. Exposure times for each filter are given in seconds.

sources needs better resolution to reduce its effect. Since the resolution of the HST is far superior to anything yet possible from the ground then images taken with the HST should reduce the point source contamination considerably. The HST data therefore will provide a crucial check of the accuracy of the ground-based SBF technique.

2 THE OBSERVATIONS

A search of the HST archive provided us with images of three galaxies, on which to perform the SBF analysis, with previous ground-based SBF distances which can then be checked. WFPC2 frames taken using the F814W and F555W filters were available for each of the galaxies NGC 3379, NGC 4472 and NGC 4406. The details of the frames are given in Table 1.

All of the archive frames have the nucleus of the galaxy centred on the PC chip, with the outer regions present in

^{*} Based on observations made with the NASA/ESA Hubble Space Telescope, obtained from the data archive at the Space Telescope Science Institute. STScI is operated by the Association of Universities for Research in Astronomy, Inc. under the NASA contract NAS 5-26555.

all of the WF chips. On none of the frames were the central regions of the galaxy saturated.

3 DATA REDUCTION

All of the data were reduced using software available under IRAF[†] and some specially written software by the authors. The frames for each galaxy and filter were co-added and any cosmic rays removed using the standard tools available under IRAF in the STSDAS package.

3.1 Removing the galaxy background

Before we are able to investigate the SBF, the galaxy background needs to be removed from the images.

For the PC images an ellipse fitting routine was used (*ellipse* under the *stsdas.analysis.isophote* package). This routine iteratively fits elliptical isophotes over a 2-dimensional image and produces an output which can be used to construct a smooth image of the fit. This image was then subtracted from the original image to give a resultant image which is flat on large scales. Generally the fitting worked well, but very close into the nucleus of the galaxy it failed. For some PC images the fitting broke down completely at the edges of the chip.

For the WF images it was not possible to use any of the ellipse fitting routines available under IRAF since they all required that the center of the ellipse was in the image. Instead, we followed Simard & Pritchett (1994) and used *fit1d* to provide a fit to the galaxy background. For each frame thirty *fit1d* passes were made with five 2.5σ rejection iterations for each pass. For all the WF frames this provided a flat image, except for the bottom ≈ 200 pixels of each frame where the subtracted image showed some structure.

3.2 Detection and removal of point sources

Once a flat image was obtained, DAOPHOT was used to find all sources greater than 4 sigma above the background and determine their magnitudes. To determine the magnitude of the point sources aperture photometry was used, with an aperture radius of $0.''5$. Crowding was not a problem on any of the frames. After zero-pointing the magnitudes of the point sources using the method described in Holtzman *et al* (1995), a point source number count was then constructed using 0.5mag bins down to the completeness limit of the data.

The sum of a Gaussian globular cluster luminosity function (GCLF) (Harris 1988) and a power-law number count for background galaxies was then fitted to the observed point source number count. For the GCLF $\sigma = 1.4\text{ mag}$ was adopted and $M_0^V = -7.4$ (Harris 1988). For the background galaxies the slope and zero-point of the number count was found by combining I band counts from a variety of sources (Tyson 1988; Lilly *et al* 1991; Driver *et al* 1994; Hall & Mackay 1984; Koo 1986; Glazebrook *et al* 1995; Smail *et al* 1996; Driver *et al* 1995) and then fitting a power law to

the combined counts (see Figure 1). This gave a slope of 0.322 ± 0.005 for the I band counts, with an intercept of -3.158 ± 0.122 . The galaxy number count was fixed, as was the apparent magnitude of the GCLF, while the amplitude of the GCLF was allowed to vary to provide the best fit. The apparent magnitude of the peak of the GCLF was first set by the distances given in Ciardullo *et al* (1993) for each galaxy, then determining the distance to the galaxy using the HST data, recalculating the peak based on the new distances, and then iterating.

Once the best fit to the point source number count was determined it was then possible to calculate the contribution to the variance in the image that point sources beyond our cutoff magnitude ($I_{KC} \sim 24\text{mag}$) make. This was done by integrating the fitted number count past the cutoff, using the equation for the residual power P_r

$$P_r = \sum n(m)f^2(m)/\bar{g} \quad (1)$$

where $n(m)$ is number of undetected point sources per pixel in the magnitude bin centred on m , $f(m)$ is the flux of a source of magnitude m and \bar{g} is the average galaxy flux per pixel.

3.3 Determining the SBF power by Fourier analysis

To determine the power present in the image due to SBF signal it is necessary to construct a Fourier power spectrum of the image. Since the SBF signal has the effect of the point spread function (PSF) of the telescope/detector imprinted on it, it is possible to separate it from the other sources of variance (shot noise, readout noise) that appear as white noise in the power spectrum (*i.e.* equal power at all scales).

Before the power spectrum is found for the image, a mask image is constructed. The mask image is 1 everywhere except for areas of 20 by 20 pixels, which are set to zero, centred on the positions of all point sources down to the magnitude limit used above to calculate the number count. Also, any defects and, in the case of the PC chips, the central regions of the galaxy were masked out.

The image was then multiplied by the mask, and the observed Fourier power spectrum ($P(k)$) calculated for the masked image, using the *powerspec* task available under STSDAS/IRAF. The output power spectrum was normalised by the mean galaxy flux of the unmasked pixels in the image.

An expectation power spectrum $E(k)$ was constructed for each region by convolving the power spectrum of the PSF with the power spectrum of the mask for that region. The PSF for each region was determined by using a grid of artificial PSFs provided by Tanvir (private communication), who used the *Tiny Tim* (Kirst 1994) program to calculate artificial PSFs. In regions where bright stars were present the power spectra of the stars were found and compared to the power spectrum from the artificial PSFs. The agreement was found to be extremely good. The expectation power spectrum were normalised so that $E(k=0) = 1$. For each of the images under study the observed power spectrum was fitted using the relationship

$$P(k) = P_0E(k) + P_1 \quad (2)$$

[†] IRAF is distributed by the National Optical Astronomical Observatories

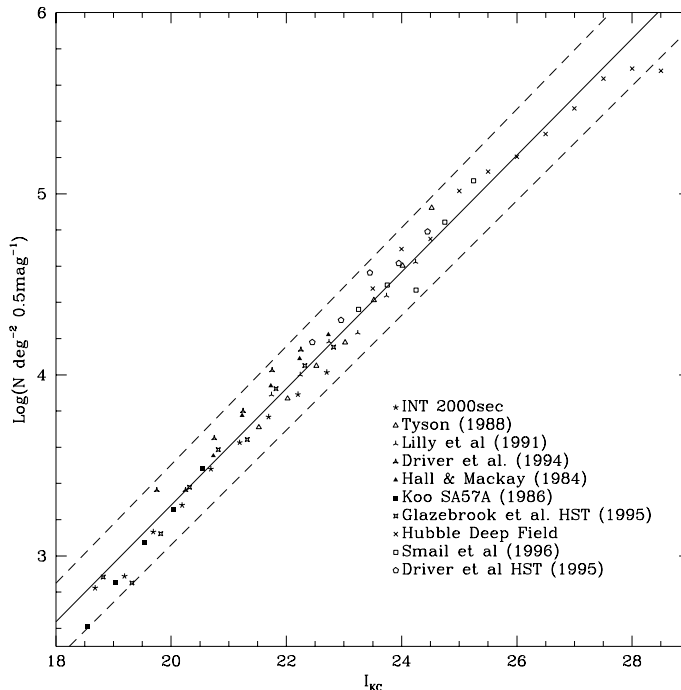


Figure 1. Galaxy counts taken from a range of sources. All magnitudes have been converted to I_{KC} and have been de-reddened. The straight line is the best least squares fit to all of the data points. The dashed lines show the error limit of the fit.

where P_0 is the sum of the the power in the image due to SBF and residual point sources, *i.e.* $P_0 = P_{fluc} + P_r$

To be able to fit the data using Equation (2), the two dimensional power spectra (as output from the 2D Fourier analysis) were converted into one dimensional power spectra by azimuthally averaging each region — each region was deliberately made square to make this task easier. The expectation power spectrum was then fitted to $P(k)$ using an iterative least squares method over several ranges of wave numbers (typically $40 < k < 70, 70 < k < 100, 100 < k < 130, 130 < k < 160, 160 < k < 190$) and a weighted average values of the parameters P_0 and P_1 calculated. This method was used so that the stability of the fits could be tested over the range of the power spectrum. Examples of the power spectra obtained and the fits calculated in the spectra are shown in Figure 2.

3.4 Comparison of observed P_1 values with theory

As a check on the fitting of the power spectrum and also the method we have used, it is possible to check the observed value of P_1 with that expected from the theory of SBF.

From Tonry & Scheider (1988) P_1 is given in their Equation 23 as

$$P_1 = \sum \sigma_R^2 + \sum \sigma_p^2 \quad (3)$$

where

$$\sigma_R^2 = N_R^2/a^2 \quad (4)$$

and

$$\sigma_p^2 = \bar{c}/a \quad (5)$$

Galaxy	Chip	Predicted P_1	Observed P_1
NGC 4472	WF2	0.103	0.095
	WF3	0.080	0.080
NGC 4406	WF2	0.068	0.058
	WF3	0.062	0.071
	WF4	0.064	0.062
NGC 3379	WF2	0.034	0.047
	WF3	0.027	0.060

Table 2. A comparison of the measured and predicted values for P_1 . All values of P_1 are given in ADU.

where a is the gain in electrons per ADU, N_R is the readout noise in electrons and \bar{c} is the mean value of the sky plus galaxy for the image. In the case of WFPC2, $a = 7$ and $N_R = 5$ which gives $\sigma_R^2 = 0.0104\text{ADU}$. For all the galaxies here, multiple frames have been averaged together, so that the observed P_1 will actually be $P_1/\sqrt{N_{frames}}$. A comparison of the observed and predicted values for P_1 is given in Table 2. As can be seen from this table there is good agreement between the theory and observations for the galaxies under study.

3.5 The effect of binning the images

To investigate whether the pixel size had any effect on the results obtained, we took several images and binned them by various factors and then performed the complete SBF analysis on the binned images. The results are shown in

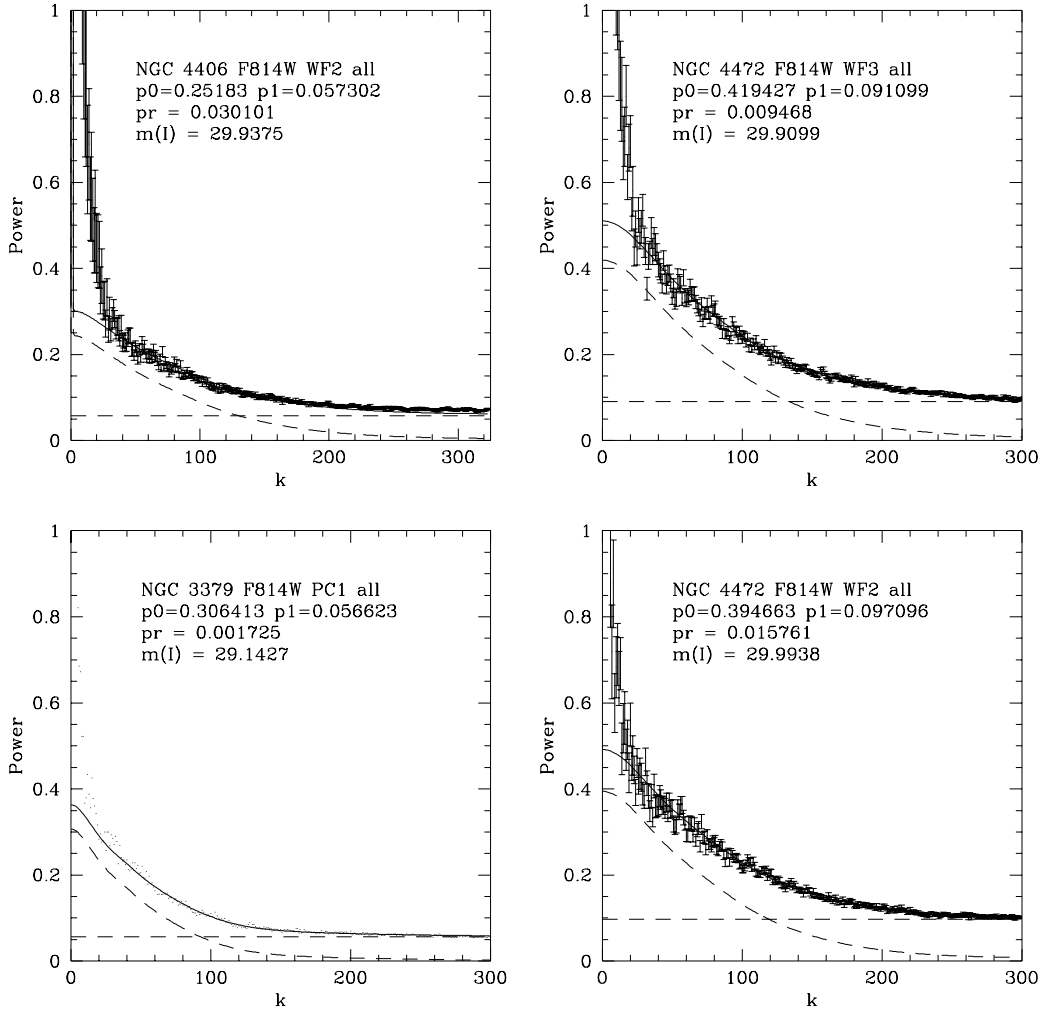


Figure 2. The observed power spectra and fitted PSF power spectra for four HST frames. The points represent the observed power spectra, the straight dashed line is P_1 and the curved dashed line is $P_0E(k)$, the scaled PSF power spectrum. The solid line is the sum of these two, i.e. $P_0E(k) + P_1$, where P_1 and P_0 are the best fit values to the data. No error bars are shown for one plot so that the scatter about the fitted line can be seen.

Galaxy	Chip	Bin Size	$(M - m)_0$
NGC 4472	WF2	1x1	31.01
		2x2	31.06
		4x4	31.27
NGC 3379	WF2	1x1	30.28
		2x2	30.37
		3x3	30.33

Table 3. The effects on $(M - m)_0$ of binning several images by different amounts.

Table 3 and show that this does not significantly change our results.

3.6 Galaxy colours

The absolute SBF magnitude is strongly dependent on the colour of the galaxy under study (see Equation 7), hence the colour needs to be determined accurately. To determine the colour, $(V-I)$, for the regions observed we used the fits to the galaxy background in both filters. The fits were then multiplied by the mask image, and the mean flux found for the unmasked pixels in the region used. To determine values for the sky flux, the median value was found in the corner of each frame furthest from the centre of the galaxy. Then, using Equation (8) and the values in Table 7 in Holtzman *et al* (1995) and an interactive method, the standard V, I and $(V-I)$ magnitudes were calculated.

Quantity	Approximate Error
P_1	$\pm 8\%$
P_R	$\pm P_R/2$
HST zero-point (V-I)	$\pm 2\%$ $\pm 5\%$

Table 4. Sources of errors in final distance modulus. The error for P_R is difficult to estimate, so we have taken it to be half the value of P_R . The error in the HST zero-point has been taken from Holtzman *et al* (1995).

4 SIMULATIONS

To confirm that the method that was used is valid simulations of all of the galaxies were performed. For each of the galaxies studied we took the galaxy fit for the WF2 frame and to this added simulated surface brightness fluctuations by adding to each pixel in the frame a random Gaussian deviate, with the variance given by Equation 10 from Tonry & Schneider (1988) and reproduced here,

$$\sigma_L^2 = \bar{g}(x, y)t \frac{10pc^2}{d} 10^{-0.4(\bar{M}-m_1)} \quad (6)$$

where σ_L^2 is the SBF variance, $\bar{g}(x, y)$ is the galaxy signal in ADU at (x, y) , t is the exposure time in seconds, d is the distance to the galaxy in parsecs, \bar{M} is the absolute fluctuation magnitude for the galaxy and m_1 is the magnitude of an object that produces 1 ADU s^{-1} on the detector/telescope used. After adding the SBF variance to the galaxy background, the whole image was then convolved with a PSF for the image, using the *fconvolve* STSDAS IRAF task. Photon and read noise appropriate for the WFPC2 was then added, to create the final simulated image. No point sources/ background galaxies were added to the image.

The simulated frames were then reduced in the same manner as the real frames, except that no point source number counts were calculated and the mask images were the same as those used for the real data. For all the simulations performed the recovered distant modulus agreed with the input distance modulus to within 0.05 mag.

5 ERROR ANALYSIS

The error in the final distance modulus was determined by evaluating the errors at all of the stages of the reduction and adding the individual errors in quadrature. The sources and representative values are shown in Table 4.

6 SBF DISTANCES

Once the colour and P_{fluc} have been determined for each of the images, it is then possible to determine the distance modulus. The absolute fluctuation magnitude (\bar{M}_I) is a function of the galaxies colour, and the dependence has been calibrated by Tonry (1991), with the dependence given by

$$\bar{M}_I = -4.84 + 3(V - I)_0 \quad (7)$$

Hence the distance modulus is given by

Galaxy	A_B
NGC 3379	0.05
NGC 4406	0.11
NGC 4472	0.00

Table 5. Foreground extinction values used for each galaxy, taken from CJT.

Galaxy	Chip	m_{fluc}	$(V - I)_{obs}$	$(m - M)_0$
NGC 3379	PC1	29.15 ± 0.10	1.24 ± 0.05	30.32 ± 0.18
	WF2	29.27 ± 0.18	1.29 ± 0.05	30.28 ± 0.23
	WF3	29.57 ± 0.28	1.28 ± 0.05	30.61 ± 0.32
	WF4	29.42 ± 0.09	1.17 ± 0.05	30.78 ± 0.18
	mean weighted	29.35 ± 0.09 29.31 ± 0.06	1.24 ± 0.03	30.50 ± 0.12 30.50 ± 0.11
NGC 4472	PC1	29.92 ± 0.10	1.26 ± 0.05	30.99 ± 0.18
	WF2	29.99 ± 0.14	1.27 ± 0.05	31.01 ± 0.21
	WF3	29.91 ± 0.20	1.29 ± 0.05	30.87 ± 0.25
	mean weighted	29.94 ± 0.08 29.94 ± 0.08	1.27 ± 0.01	30.96 ± 0.09 30.97 ± 0.12
	NGC 4406	PC1	29.85 ± 0.06	1.27 ± 0.05
WF2		29.94 ± 0.31	1.21 ± 0.05	31.24 ± 0.34
WF3		30.22 ± 0.12	1.32 ± 0.05	31.20 ± 0.19
WF4		30.28 ± 0.22	1.23 ± 0.05	31.54 ± 0.27
mean weighted		30.07 ± 0.10 29.94 ± 0.05	1.26 ± 0.03	31.24 ± 0.12 31.16 ± 0.11

Table 6. Results of the SBF analysis for all three galaxies. m_{fluc} and V-I are both uncorrected for absorption. The measurement errors on individual frames are estimated as indicated in Table 4. The errors on the mean are estimated from the rms variation between frames in the cases of NGC3379 and NGC4406 and from the average instrumental errors added in quadrature in the case of NGC4472. The weighted means (and errors) are calculated using the measurement errors shown for each individual frame.

$$(m - M)_0 = m_{fluc} + 4.84 - 3(V - I)_{obs} + 0.80A_B \quad (8)$$

where m_{fluc} is the apparent fluctuation magnitude and A_B is the absorption present (this is Equation 3 from Ciardullo *et al* (1993, hereafter referred to as CJT)). For each galaxy we have used the values of A_B (see Table 5) given in CJT, which were derived from Burstein & Heiles (1984) and Burstein *et al* (1987). The results for each galaxy are given in Tables 6 and a comparison of the results for m_{fluc} with previous ground based results is given in Table 7, and shown graphically in Figure 3.

7 COMPARISON WITH SBF RESULTS OF CIARDULLO ET AL, 1993

By comparing the unweighted and weighted errors in Table 6, we see that the r.m.s. spread in the values of m_{fluc} and $(m - M)_0$ for our observations is consistent with the calculated errors from the fitting of the power-spectrum and measuring V-I. The average (weighted) final values of $(m - M)_0$ for each galaxy have an error of order ± 0.12 mag, indicating

Galaxy	m_{fluc} (this)	m_{fluc} (CJT)	diff
NGC 3379	29.31 ± 0.06	28.65 ± 0.07	0.66 ± 0.09
NGC 4472	29.94 ± 0.08	29.66 ± 0.07	0.28 ± 0.11
NGC 4406	29.94 ± 0.05	29.97 ± 0.07	-0.03 ± 0.09
Galaxy	$(m - M)_0$ (this/CJT)	$(m - M)_0$ (CJT)	diff
NGC 3379	30.50 ± 0.11	29.87 ± 0.07	0.63 ± 0.13
NGC 4472	30.97 ± 0.12	30.78 ± 0.07	0.19 ± 0.14
NGC 4406	31.16 ± 0.11	31.24 ± 0.08	-0.08 ± 0.14
	Mean offsets		0.25 ± 0.21
	r.m.s. error		± 0.36
Galaxy	$(m - M)_0$ (this/TBAD)	$(m - M)_0$ (CJT)	diff
NGC 3379	30.73 ± 0.24	30.14 ± 0.07	0.59 ± 0.25
NGC 4472	31.13 ± 0.24	31.00 ± 0.07	0.13 ± 0.25
NGC 4406	31.48 ± 0.25	31.55 ± 0.08	-0.07 ± 0.26
	Mean offsets		0.22 ± 0.20
	r.m.s. error		± 0.35

Table 7. A comparison of the SBF fluctuation magnitudes and distance moduli (assuming the $M_I : V-I$ calibration of CJT) presented here and those previously determined from ground based observations taken from CJT. m_{fluc} is uncorrected for absorption. The final three rows are the values for $(m - M)_0$ using the new calibration of M_I with $(V-I)$ given by Tonry *et al* (1997, denoted by TBAD) and with slope -4.5. For individual galaxies, weighted means and errors for all quantities are quoted. The mean offsets and errors are unweighted, with the error here being on the mean and the figure in brackets being the error on an individual galaxy offset.

that our HST SBF measures provide distances with reasonable internal accuracy.

Table 7 shows that there is a significant, 4.8σ , disagreement between our result for the distance modulus of NGC 3379 and that of CJT. There is a less significant disagreement over the distance of NGC 4472 and the distance for NGC 4406 is consistent with that given by CJT. Table 7 and Figure 3 shows that, on average, the CJT distances are about 12% less than ours. However, given at least our error estimates for the HST SBF method, this offset is insignificant. Table 7 and Figure 3 also show that the scatter around the mean offset, (dashed) line is larger than that expected from the claimed errors of CJT. Of course, the scatter around the 1-1, (solid) line is even larger. Table 7 confirms that the rms scatter between the results is ± 0.36 mag compared to an expected scatter of ± 0.14 mag from our error estimates and those of CJT. There may also be some indication of non-linearity between the HST and ground-based distance estimates, though more HST SBF measurements are needed before this can be taken as established.

The most obvious candidate for the cause of differences between the HST and ground-based results is point source removal. With the much higher resolution of the HST, one should do much better at point source detection and removal. However, Figure 4 shows a comparison of the density of point source detected in the WF2 (scaled to correct for different pixel sizes) frame of NGC 4472 compared to the point source number counts given in Tonry *et al* (1990, hereafter

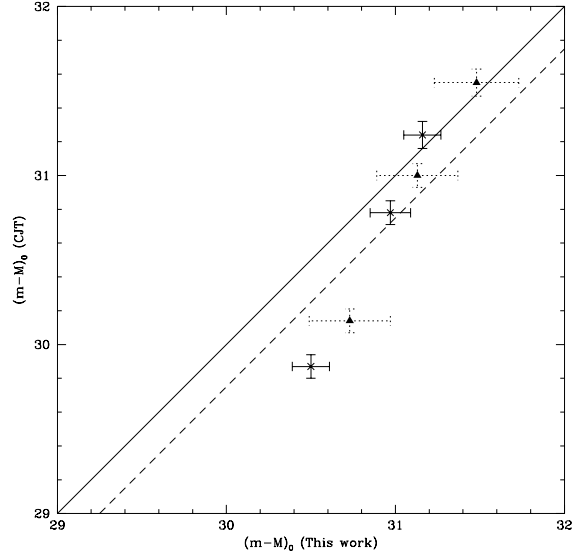


Figure 3. A comparison of our results for $(m - M)_0$ with those published in CJT. The solid line shows the 1:1 relationship, while the dashed line is offset by the mean difference between our results and CJT's. The observed dispersion around the solid 1:1 line is much bigger than the statistical errors would imply. Even around the dashed line, which is shifted by 0.25mag to represent the mean difference between CJT and ourselves, the observed dispersion is much larger than expected. The triangles with the dotted error bars are when the distances are calculated using the new calibration given by Tonry *et al* (1997).

referred to as TAL). As can be seen, in this case at least, the agreement between the point source counts is very good.

One difference with our methodology is that, to estimate P_r , TAL have taken the galaxy count slope for the I band from Harris (1988), which gives a value of 0.34. Although this slope is therefore steeper than the value we have used, Figure 4 actually shows that, in the case of NGC4472, their galaxy number count lies significantly below that used here because our zero-point offset is higher than CJT's. If CJT use our galaxy counts their values of P_r will be increased. Therefore, if the same situation applies for for NGC 3379, the discrepancy there could be due to CJT using an underestimate of the galaxy counts within the field. Unfortunately, for NGC 3379 and NGC 4406 it is not possible to determine whether the same arguments apply because CJT's point source count fits in these cases are not published.

The only way we can reduce our distance for NGC3379 to improve agreement with CJT is by **not** subtracting from P_0 any background point source contribution to the variance (*i.e.* set $P_r = 0$), but even this does not eliminate the large difference — at most it decreases our values of $(m - M)_0$ by 0.06 mag. Therefore, the discrepancy between CJT and ourselves cannot be due to any overestimate we have made of the background counts, since even setting $P_r=0$ only reduces the HST NGC3379 distance modulus by a negligible amount.

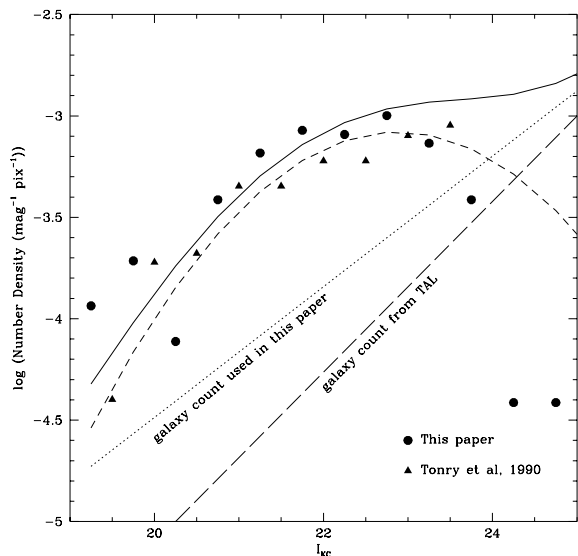


Figure 4. Point source densities in the WF2 field for NGC 4472 compared to those given by TAL. The values from this work have been scaled to 0.29 arcsecond pixel size of TAL. The solid line is the fit to the point source number count as the sum of the galaxy number count (power law, shown by the dotted line) and a globular cluster luminosity function (a gaussian shown as a short dashed line). The dashed line is the galaxy number count used by TAL.

7.1 Effects of the new $M_I : (V - I)$ calibration

In Tonry *et al* (1997) a quite different calibration of M_I with $(V - I)$ is given as

$$\overline{M}_I = -1.74 + 4.5((V - I)_0 - 1.15) \quad (9)$$

Taking into account the effects of absorption this implies that the distance modulus is given by

$$(m - M)_0 = m_{fluc} + 1.74 - 4.5((V - I)_{obs} - 1.15) + 1.39A_B \quad (10)$$

The results of the new calibration are given in Table 7 and shown graphically in Figure 3. With this new calibration the mean difference between our results and those of CJT is only slightly reduced to 0.22 mag from 0.25 mag because only the zero-point is changed. There is also no significant improvement in the scatter between our and CJT's results with the r.m.s. error now ± 0.35 mag for an individual galaxy, compared to an expected error of ± 0.25 mag (see Table 7).

8 COMPARISON WITH HST SBF RESULTS OF AJHAR ET AL 1997

After this paper was submitted, Ajhar *et al* (1997) published HST SBF results for 16 galaxies, including the 3 galaxies discussed here using the same HST data. It is therefore of interest to compare their results with ours. Ajhar *et al* only use the data from the Planetary Camera to derive their results and in Table 8 we compare the fluctuation magnitudes, V-I colours and distance moduli. Since Ajhar *et al* calibrate their HST SBF distances against the re-calibrated ground-based

Galaxy	PC m_{fluc} (this paper)	PC m_{fluc} (Ajhar <i>et al</i>)	diff
NGC 3379	29.25 ± 0.10	29.04 ± 0.05	0.21 ± 0.11
NGC 4472	30.02 ± 0.10	30.09 ± 0.04	-0.07 ± 0.11
NGC 4406	29.95 ± 0.06	30.06 ± 0.05	-0.11 ± 0.08
	Mean offset		0.01 ± 0.10
	r.m.s. error		± 0.17
Galaxy	PC $(V - I)_{obs}$ (this paper)	PC $(V - I)_{obs}$ (Ajhar <i>et al</i>)	diff
NGC 3379	1.24 ± 0.05	1.260 ± 0.006	-0.020 ± 0.05
NGC 4472	1.26 ± 0.05	1.292 ± 0.012	-0.032 ± 0.05
NGC 4406	1.27 ± 0.05	1.255 ± 0.011	0.015 ± 0.05
	Mean offset		-0.01 ± 0.014
	r.m.s. error		± 0.024
Galaxy	PC $(m - M)_0$ (this paper)	PC $(m - M)_0$ (Ajhar <i>et al</i>)	diff
NGC 3379	30.46 ± 0.34	30.13 ± 0.063	0.33 ± 0.35
NGC 4472	31.04 ± 0.34	30.90 ± 0.088	0.14 ± 0.35
NGC 4406	31.05 ± 0.33	31.26 ± 0.094	-0.21 ± 0.34
	Mean offset		0.09 ± 0.16
	r.m.s. error		± 0.27

Table 8. A comparison of the observed PC fluctuation magnitudes, V-I colours and distance moduli from our analysis and from the analysis of Ajhar *et al* (1997) using the same HST data. 0.1mag has now been added to our fluctuation magnitudes and distance moduli to make our HST zeropoint consistent with that of Ajhar *et al*. The final three rows include our values for $(m - M)_0$ assuming the HST calibration of M_I with $(V - I)$ given by Ajhar *et al* (1997) with a V-I coefficient of -6.5.

distances of Tonry *et al* (1997), the new distance moduli for these 3 galaxies are 0.13 ± 0.07 mag bigger than for CJT, reflecting the increase in the Tonry *et al* (1997) distance modulus calibration over that of CJT.

Now it should first be noted that for the same PC data the two sets of results are closely similar. In particular, for NGC3379 the fluctuation magnitude of Ajhar *et al* has increased to lie within 0.21 mag of our PC value. In the mean, Table 8 shows that the fluctuation magnitude difference is only 0.01 ± 0.10 (0.17) mag and the observed V-I colour difference is only -0.01 ± 0.014 (0.024) mag. The figures in brackets represent the estimated r.m.s error on each individual difference. Dividing these by $\sqrt{2}$, suggests that the error on each fluctuation magnitude is ± 0.12 mag and on each $V - I$ colour is ± 0.017 mag. The error on an individual difference in $(m - M)_0$ is ± 0.27 mag with the error being approximately equally distributed between the colour and the fluctuation magnitude errors. Thus although the systematic differences between the two analyses are small, the errors on individual measurements are non-negligible at ± 0.12 mag and ± 0.19 mag on individual measurement of m_{fluc} and $(m - M)_0$ and closer to our error estimates than those of Ajhar *et al*. However, the level of disagreement in measuring m_{fluc} at ± 0.17 mag is too small to explain the large, ± 0.25 mag, scatter seen in the previous comparison with the results of CJT in Table 7.

Table 9 further compares the HST distance moduli of Ajhar *et al* (1997) and our results, these also now including the three WF camera frames, as well as the PC frame.

Table 9 also intercompares our results with the new ground-based SBF distance moduli of Tonry *et al* (1997), published for the first time by Ajhar *et al* (1997). Taking the top two sets of rows first, where our results now assume the new, steep slope (-6.5), HST $M_I : V - I$ calibration of Ajhar *et al* with we first note that although the systematic errors in the mean remain insignificant, the rms errors in the individual $(m - M)_0$ differences have now increased to ± 0.42 mag in the case of the Ajhar *et al* data and to ± 0.43 mag in the case of the Tonry *et al* data. In the case of NGC3379, the previous 0.33 mag discrepancy in the PC $(m - M)_0$ has increased to 0.65 mag. This is because our overall fluctuation magnitude has increased by a further 0.16 mag and this has not been offset by any increase in V-I colour; indeed the reverse is true particularly in the case of chip WF4 (see Table 7.)

In general, there is no evidence in the correlation between our results for the four HST frames that the new steep HST $M_I : V - I$ calibration with slope -6.5 (Ajhar *et al* 1997) leads to a smaller dispersion in distance; indeed there is clear evidence that it increases it (see Table 9.), since our errors in $(m - M)_0$ significantly increase when this relation is used rather than that of CJT (see bottom two sets of rows in Table 9). It is unlikely that this is just due to our own measurement errors since the agreement in V-I between ourselves and Ajhar *et al* for the PC V-I colour is good with the error being -0.012 ± 0.014 (0.024) mag and this is generally much smaller than the dispersion in colour between the four WFPC2 CCDs (± 0.054 mag for NGC3379, ± 0.049 mag for NGC4406, ± 0.015 mag for NGC4472). The suggestion is that either the intrinsic V-I measurement errors in the HST data are much larger than claimed by Ajhar *et al* or the correlation between m_{fluc} and colour for the HST bands is much less steep than they claim.

The comparison of our 4-frame result with the 1-frame result of Ajhar *et al* in the third set of rows in Table 9 also shows that the r.m.s. differences at ± 0.24 mag for each galaxy are reduced from those found in our comparison with the previous ground-based results of CJT (± 0.36 mag). Splitting this error equally between Ajhar *et al* and ourselves would give an estimated ± 0.17 mag error on an individual HST SBF measurement. However, the r.m.s. difference at ± 0.24 mag is still significantly bigger than indicated by combining our formal SBF measurement error at $\sim \pm 0.12$ mag with that of Ajhar *et al* at $\sim \pm 0.08$ mag. The comparison of our HST SBF moduli with the new ground-based moduli of Tonry *et al* 1997 in the final set of rows in Table 9 leads to similar conclusions.

Ajhar *et al* (1997) also concluded that measurement errors alone were not enough to explain the dispersion between their new ground-based and HST observations. However, the final average, *total* error of ± 0.12 mag quoted by them for their HST SBF distance moduli is still lower than we derive. If the galaxy NGC4621, classed as an ‘outlier’, is re-included in their sample, then their total error on each HST distance modulus rises to ± 0.17 mag which is close to what we estimate.

Thus, overall, the analyses of Ajhar *et al* and ourselves seem to show reasonable agreement in m_{fluc} and V-I measurements in the PC images of these three galaxies. They also verify that the measurement errors on these quantities are consistent with our estimates. However, significant disagreements remain between our overall HST SBF results

Galaxy	$(m - M)_0$ (this/HST)	$(m - M)_0$ (Ajhar <i>et al</i> 97)	diff
NGC 3379	30.78 ± 0.33	30.13 ± 0.063	0.65 ± 0.34
NGC 4472	30.95 ± 0.33	30.90 ± 0.088	0.05 ± 0.34
NGC 4406	31.11 ± 0.33	31.26 ± 0.094	-0.15 ± 0.34
	Mean offsets		0.18 ± 0.24
	r.m.s. error		± 0.42
Galaxy	$(m - M)_0$ (this/HST)	$(m - M)_0$ (Tonry <i>et al</i> 97)	diff
NGC 3379	30.78 ± 0.33	30.08 ± 0.080	0.70 ± 0.34
NGC 4472	30.95 ± 0.33	30.94 ± 0.068	0.01 ± 0.34
NGC 4406	31.11 ± 0.33	31.19 ± 0.070	-0.08 ± 0.34
	Mean offsets		0.21 ± 0.25
	r.m.s. error		± 0.43
Galaxy	$(m - M)_0$ (this/CJT)	$(m - M)_0$ (Ajhar <i>et al</i> 97)	diff
NGC 3379	30.50 ± 0.11	30.13 ± 0.063	0.37 ± 0.13
NGC 4472	30.97 ± 0.12	30.90 ± 0.088	0.07 ± 0.15
NGC 4406	31.16 ± 0.11	31.26 ± 0.094	-0.10 ± 0.14
	Mean offsets		0.11 ± 0.14
	r.m.s. error		± 0.24
Galaxy	$(m - M)_0$ (this/CJT)	$(m - M)_0$ (Tonry <i>et al</i> 97)	diff
NGC 3379	30.50 ± 0.11	30.08 ± 0.080	0.42 ± 0.14
NGC 4472	30.97 ± 0.12	30.94 ± 0.068	0.03 ± 0.14
NGC 4406	31.16 ± 0.11	31.19 ± 0.070	-0.03 ± 0.13
	Mean offsets		0.14 ± 0.14
	r.m.s. error		± 0.24

Table 9. A comparison our HST (WF+PC) distance moduli calibrated using either the HST $M_I : V - I$ calibration of Ajhar *et al* (1997) or the original calibration of CJT as indicated, with the HST results of Ajhar *et al* and the ground-based results of Tonry *et al* (1997). Again, in the top two sets of rows where our results assume the HST calibration of Ajhar *et al*, we have increased our distance moduli by 0.1 mag to be consistent with their HST zeropointing procedure.

and the HST and ground-based SBF results of Ajhar *et al* which suggest that the errors on the SBF method may be significantly larger than expected from simply combining measurement errors.

9 CONCLUSIONS

We have discovered a disagreement between HST SBF distances and those previously determined by CJT using ground-based images. In the case of one galaxy, NGC 3379, the discrepancy is 0.63 ± 0.13 mag and is significant at the 4.8σ level. From the overall comparison, the real error on the ground-based SBF distance moduli of CJT could be as high as ± 0.25 mag on average, compared to the ± 0.08 mag claimed by CJT from measurement errors. A possible cause of the disagreement in the case of NGC3379 is that the error associated with the background galaxy correction has been underestimated by CJT; our HST results are insensitive to this type of error.

Improved agreement is seen with the HST SBF results of Ajhar *et al* (1997) and the new ground-based results of

Tonry *et al* (1997). In particular, on the same individual HST PC frame, the results of Ajhar *et al* and ourselves for m_{fluc} agree to ± 0.17 mag and for V-I to ± 0.017 mag. In the case of the distance modulus, the comparison of our 4-frame HST results with both the above HST and ground-based results suggest that the error is probably reduced to ± 0.17 mag for an individual galaxy distance modulus. However, this is still significantly larger than claimed by these authors. Also, we find no evidence in our WFPC2 data to support the steep slope of -6.5 for the HST $M_I : V - I$ relation advocated by Ajhar *et al* (1997). Further, since the HST data of Ajhar *et al* is a subset of that used here, these two results are not independent and the real error on HST SBF distance estimates could be larger. Finally, it should be noted that the error estimates presented here form a lower limit to the true SBF error because all points of comparison accept the precepts of the SBF method and make no reference to independent methods of distance estimation.

REFERENCES

- Ajhar, E.A., Lauer, T.R., Tonry, J.L., Blakeslee, J.P., Dressler, A., Holtzman, J.A., Postman, M., 1997, AJ, **114**,626
 Burstein, D., and Heiles, C., 1984, ApJS, **54**, 33
 Burstein, D., Davies, R.L., Dressler, A., Faber, S.M., Stone, R.P.S., Lynden-Bell, D., Terlevich, R.J., and Wagner, G., 1987, ApJS, **64**, 601
 Ciardullo, R., Jacoby, G.H., and Tonry, J.L., 1993, ApJ, **419**, 479
 Driver, S.P., Phillipps, S., Davies, J.I., Morgan, I., and Disney, M.J., 1994, MNRAS, **226**, 155
 Driver, S.P., Windhorst, R.A., Ostrander, E.J., Keel, W.C., Griffiths, R.E., Ratnatunga, K.U., 1995, ApJ, **449**, 23
 Glazebrook, K., Ellis, R., Colless, M., Broadhurst, T., Allington-Smith, J., and Tanvir, N., 1995, MNRAS, **273**, 157
 Hall, P., and Mackay, C.D., 1984, MNRAS, **210**, 979
 Harris, W.E., 1988, in *The Extragalactic Distance Scale*, ASP Conference Series, Vol. 4, edited by S. van den Bergh and C.J. Pritchet
 Holtzman, J.A., Burrows, C.J., Casertano, S., Hester, J.J., Trauger, J.T., Watson, A.M., and Worthey, G., 1995, PASP, **107**, 1065
 Kirst, J., 1994, *The Tiny Tim User's Manual*, version 4.0
 Koo, D.C., 1986, ApJ, **311**, 651
 Lilly, S.J., Cowie, L.L., and Gardner, J.P., 1991, ApJ, **369**, 79
 Simard, L., and Pritchet, C.J., 1994, AJ, **107**, 503
 Smail, I., Dressler, A., Kneib, J., Ellis, R.S., Couch, W.J., Sharples, R.M., and Oemler, A.Jr, 1996, ApJ, **469**, 508
 Tonry, J., Ajhar, E.A., Luppino, G.A., 1990, AJ, **100**, 1416
 Tonry, J., 1991, ApJ, **373**, L1
 Tonry, J., and Schneider, D.P., 1988, AJ, **96**, 807
 Tonry, J., Blakeslee, J.P., Ajhar, E.A., and Dressler, A., 1997, ApJ, **475**, 399
 Tyson, J.A., 1988, AJ, **96**, 1